The Astrophysical Journal, 602:545–554, 2004 February 20

THE DISTRIBUTION OF Lyα-EMITTING GALAXIES AT $z = 2.38$[1]

Povilas Palunas,[2] Harry I. Teplitz,[3] Paul J. Francis,[4,5] Gerard M. Williger,[6,7] and Bruce E. Woodgate[6]

Received 2003 August 25; accepted 2003 October 21

ABSTRACT

We present the detection of 34 Lyα emission-line galaxy candidates in a $80 \times 80 \times 60$ comoving Mpc region surrounding the known $z = 2.38$ galaxy cluster J2143−4423. The space density of Lyα emitters is comparable to that found by Steidel et al. when targeting a cluster at redshift 3.09, which is a factor of 5.8 ± 2.5 greater than that found by field samples at similar redshifts. The distribution of these galaxy candidates contains several 5–10 Mpc scale voids. We compare our observations with mock catalogs derived from the VIRGO consortium ΛCDM *n*-body simulations. Fewer than 1% of the mock catalogs contain voids as large as we observe. Our observations thus tentatively suggest that the galaxy distribution at redshift 2.38 contains larger voids than predicted by current models. Three of the candidate galaxies and one previously discovered galaxy have the large luminosities and extended morphologies of "Lyα blobs."

Subject headings: cosmology: observations — galaxies: evolution — galaxies: fundamental parameters

1. INTRODUCTION

The two-point correlation coefficient of high-redshift ($z > 2$) galaxies is quite similar to that of galaxies today (e.g., Steidel et al. 1996, 2000; Giavalisco et al. 1998). The *topology* of the distribution of high-redshift galaxies, however, is not yet clear. The two-point correlation coefficient alone is not very sensitive to this topology. In the local universe, a large fraction of galaxies lie in filaments and sheets, such as the Great Wall (Geller & Huchra 1989). These filaments may be several hundred Mpc in length and are separated by voids that can be tens of Mpc across. Our understanding of how and when filaments and voids were established depends on the geometry of the universe and biasing of galaxies (e.g., White & Frenk 1991; Kauffmann, Nusser, & Steinmetz 1997; Mo, Mao, & White 1999).

Mapping such large-scale structure at high redshifts requires a careful balance of field of view (to encompass the structures), redshift coverage (to accept enough test objects in the structure while avoiding confusion by overlapping structures in distance), and photometric sensitivity (to find enough test objects). Photometric redshifts (see Hogg et al. 1998 for a review) provide an efficient estimate of redshift for large imaging surveys, but they are not accurate enough to avoid confusion from multiple overlapping structures and cannot delineate the structures directly. Bright quasi-stellar objects (QSOs) may be markers of dense regions (Ellingson, Yee, & Green 1991) but are too sparse to provide multiple samples within individual structure elements.

Narrowband imaging to find Lyα-emitting galaxies has many advantages as a technique for mapping the topology of the galaxy distribution at high redshifts. The technique picks out galaxies in a narrow range of redshifts, so the two-dimensional distribution of their positions on the sky can be used to constrain the topology alone, without the need for expensive follow-up spectroscopy. At sufficiently low flux limits, the space density of detectable Lyα emitters becomes comparable to that of Lyman break galaxies (e.g., Hu & McMahon 1996). They should be dense tracers of large-scale structure. With large–format prime-focus imagers, it is relatively straightforward to survey very large volumes of the early universe. The fast beam required for large field coverage puts a lower limit the width of the narrowband filter. Typically, this limits the line-of-sight depth covered in an exposure to be roughly equal to or greater than the width. A disadvantage of Lyα searches is that the Lyα emission from a galaxy is very hard to predict theoretically because of the very high optical depth in this line, its dependency on metallicity and star formation rate, and the ease with which it can be obscured by dust.

Two studies find some evidence for filamentary structure in the distribution of Lyα-emitting galaxies on scales of around 5 Mpc (Campos et al. 1999; Møller & Fynbo 2001). Other surveys have found evidence for clustering in Lyα-emitting galaxies, but not for filamentary structure (Steidel et al. 2000; Ouchi et al. 2003).

In this paper, we present the detection of 34 candidate Lyα-emitting galaxies in a region containing J2143−4423, a $z = 2.38$ cluster of galaxies and damped Lyα absorbers (Francis et al. 1996; Francis, Woodgate, & Danks 1997, 2001b). Our survey covers a region of $80 \times 80 \times 60$ comoving Mpc in size and hence is sensitive to much larger structures than previous studies at comparable redshifts. The narrowband imaging also detects four extended nebulae of Lyα emission, often dubbed "blobs" (Steidel et al. 1998; Keel et al. 1999; Francis et al. 2001b). Throughout the paper, we assume a Λ-dominated flat universe ($H_0 = 65$ km s^{-1} Mpc^{-1}, $\Omega_M = 0.3, \Omega_\Lambda = 0.7$).

2. OBSERVATIONS AND DATA REDUCTION

The data were taken with the MOSAIC II instrument on the Blanco 4 m telescope at the Cerro Tololo Inter-American Observatory (CTIO). Observations were made on the nights of 1999 August 7–8, in the Johnson *UBV* and Cousins *RI* filters,

[1] Based on observations obtained at the Cerro Tololo Inter-American Observatory, a division of the National Optical Astronomy Observatories, which is operated by the Association of Universities for Research in Astronomy, Inc. under cooperative agreement with the National Science Foundation.

[2] McDonald Observatory, University of Texas, Austin, TX 78712.

[3] *Spitzer* Science Center, California Institute of Technology, Pasadena, CA 91125.

[4] Research School of Astronomy and Astrophysics, The Australian National University, Canberra, ACT 0200, Australia.

[5] Joint appointment with the Department of Physics, Faculty of Science.

[6] NASA Goddard Space Flight Center, Greenbelt, MD 20771.

[7] Johns Hopkins University, Baltimore, MD 21218.

TABLE 1
OBSERVATIONS

Filter	Exposure Time per Frame (s)	Number of Frames	FWHM (arcsec)	5 σ[a] (AB mag)
U	1800	5	1.49	23.9
B	600	12	1.37	26.2
V	600	12	1.37	25.3
R	600	5	1.64	24.0
I	600	5	1.11	23.8
NB	1800, 2700	5, 4	1.35	23.5

[a] The 5 σ limit for a point source, on the AB magnitude system.

and in a custom narrowband interference filter (*NB*) centered at 4107 Å with a FWHM of 54 Å. The *NB* filter was designed to image Lyα emission at $z = 2.38$ (Francis et al. 2001b). The delivered filter covers Lyα redshifts in the range $2.356 < z < 2.401$. The MOSAIC II is a prime-focus camera consisting of eight CCDs, each with 2048×4096 pixels. The camera has a plate scale of $0\farcs27$ pixel^{-1} and covers an overall area of $(36')^2$ with small $9''-13''$ gaps between the CCDs. Individual exposures were dithered by $10'$. The full *NB* integration time of 19,800 s was achieved for a $26' \times 26'$ region centered on the J2143−4423 cluster, while shorter integrations extend over a $48' \times 50'$ field. The final trimmed images are $45\farcm9 \times 45\farcm5$ in size, excluding $9' \times 9'$ in the southeast corner with only one exposure. The observations are summarized in Table 1.

This was the first science run with MOSAIC II. The readout clocking was still being tuned, and biases had a slowly varying harmonic pattern due to the beating of unsynchronized clocks. A fast Fourier transform (FFT) based algorithm was developed to subtract the ringing component of the bias. The period of the pattern was approximately 160 pixels ($120''$) in the readout direction on the CCD. Because this scale is significantly larger than the size of any source in the images, the subtraction algorithm should not affect the detection or photometry of the sources. All detections were verified in the raw images.

Further image reductions were performed using the MSCRED package in IRAF.[8] These include a correction for crosstalk between the CCDs, bias subtraction, and flat fielding.

Twilight flats were used for all of the images except for the *I* band. The *I*-band twilight flats exhibited considerable fringing, with a different pattern than that due to the night sky. The *I*-band dome flats, however, were not uniformly illuminated, and an illumination correction was derived from highly smoothed twilight flats. The *I*-band images were defringed by combining all of the images with object rejection. The objects were rejected by making a mask using the SExtractor (Bertin & Arnouts 1996) object images. The object mask images were convolved with a 20 pixel diameter top-hat kernel to reject the low surface brightness tails of the objects.

Wide-field optical distortions were corrected using a standard astrometric solution for MOSAIC II provided in IRAF. Final alignment of the images was performed by matching each image to approximately 2000 stars in the Automatic Plate Measuring Facility (APM) catalog. The alignment was good to 0.3 pixels ($0\farcs08$) rms.

Before combining the images we created bad pixel masks that included hot pixels, bad columns, and cosmic rays. Cosmic rays (CRs) were selected using the *jcrrej2* package in IRAF (Rhoads 2000). We found this package to work extremely well for finding individual cosmic rays; however, we had difficulty balancing the parameters to eliminate the faint halos associated with the cosmic-ray hits. To eliminate these, we devised a filtering algorithm, which calculated the Tookey biweight statistic (Beers, Flynn, & Gebhardt 1990) in a region around each CR and eliminated all points adjacent to the CRs that were greater than 2.5 σ from the estimated background level.

Photometric calibration was performed using 56 stars in the Landolt fields 90, 92, SA 110, and 113 (Landolt 1992). A small correction was include in the calibration to account for Galactic extinction (Schlegel, Finkbeiner, & Davis 1998). Catalogs of individual sources were compiled using SExtractor. The limiting magnitudes vary across the images. Figure 1 shows an exposure map for the *NB* imaging. The map was created by summing a set of the flat-field images scaled by exposure times and with the same offsets as the *NB* exposures. The 5 σ detection limits for pointlike objects in each color are summarized in Table 1. The *NB* filter was used as a primary detection band, with measurements made in other bands using the same apertures, in order to find objects with weak continua but strong lines. Areas that are covered by only one exposure, such as the southeast corner, are excluded from the analysis. Photometry

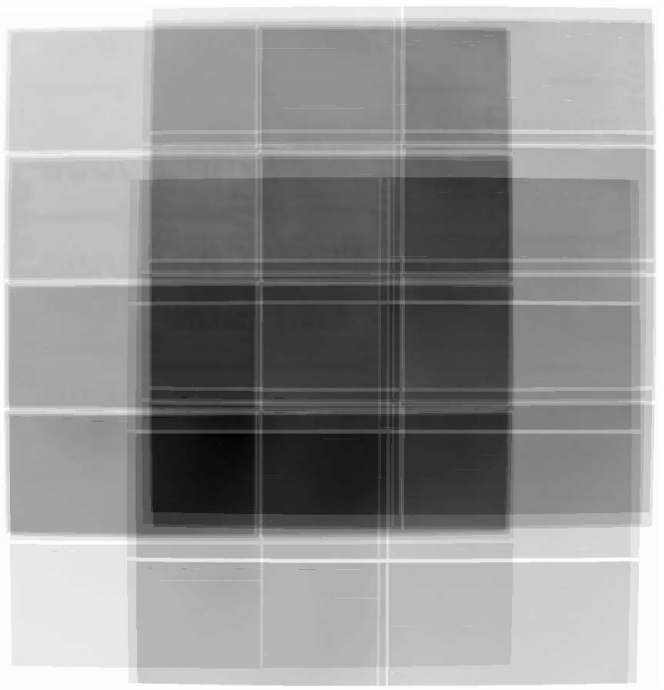

FIG. 1.—Exposure map for the *NB* imaging. North is up, and east is to the left.

[8] IRAF is distributed by NOAO, which is operated by AURA Inc., under contract to the NSF.

was measured in the Kron aperture (Kron 1980), defined as 2 times the first moment of the radial light distribution. The first moment is approximately equal to the half-light radius of the distribution. The photometric error was measured by SExtractor. Table 1 lists the 5 σ photometric sensitivity for a point source in each band.

3. RESULTS

We detect 2450 pointlike objects and 7000 resolved objects above the 5 σ limit in the *NB* filter. Lyα emitters can be identified in this sample by excess flux in the *NB* filter, compared to the continuum *B* filter. The limits for $NB-B$ color excess were determined by modeling the distribution of photometric errors in the $NB-B$ color as a function of the *NB* magnitude (see Teplitz, Malkan, & McLean 1998). The outer envelope of 5 σ errors that defines the detection limit for emission-line candidates is fitted by the function

$$[(NB - 15.25)/7.6]^4 + 0.15. \quad (1)$$

However, bright emission-line candidates with low equivalent width (EW) are more likely to be low-redshift interlopers than cluster members (see § 3.1). We consider candidates above the EW = 125 Å limit to be likely Lyα emitters. This limit is obtained as a broad minus narrowband color through the relation

$$NB - B = -2.5 \log \frac{1 + \mathrm{EW}/W_B}{1 + \mathrm{EW}/W_{NB}}, \quad (2)$$

where W_B and W_{NB} are the widths of the broad and narrowband filters.

In addition, objects that are only marginally detected in the narrowband are unlikely to be good candidates. For simplicity, we establish a uniform narrowband magnitude cut rather than base the cut on the varying depth across the image. The magnitude cut is based on the 50% completeness limit for narrowband detections (see Fig. 2).

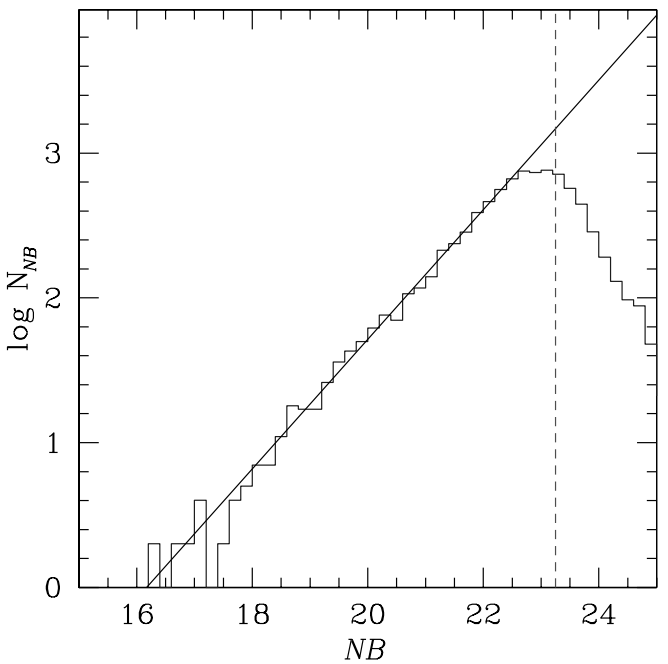

FIG. 2.—Number counts for resolved objects detected in the narrowband images. Assuming the number counts can be extrapolated by a power law, the detections are 50% complete at $NB = 23.25$.

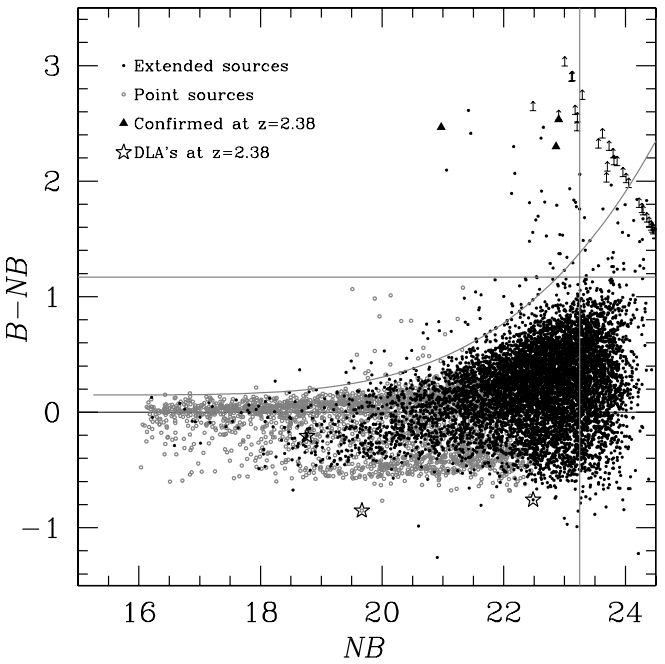

FIG. 3.—Excess flux in the *NB* filter as a function of magnitude. Black points are extended sources, and gray are unresolved sources. The large filled circles are the three spectroscopically confirmed Lyα emitters (Francis et al. 1997). Upward-pointing arrows are objects undetected in the *B*-band filter. Three damped Lyα absorbers (Francis & Hewett 1993; Francis et al. 2001b) are indicated by open stars. The curved lines indicated the 5 σ confidence level for excess emission; that is, points above the line are candidate emission-line objects. The horizontal line is the $\mathrm{EW_{obs}} = 125$ Å level. The vertical line is the 50% completeness cutoff; that is, only candidates brighter than that line are considered likely to be real. Objects that are simultaneously above the 5 σ threshold, above the observed $\mathrm{EW_{obs}} = 125$ Å level, and brighter than the 50% completeness limit are selected as Lyα emission candidates.

Figure 3 shows the $NB-B$ color excess for all objects detected in the *NB* image. The Lyα emitters from Francis et al. (1996) are clearly detected in the new *NB* measurement. For new emission-line candidates we consider objects that are detected above the 50% completeness limit in the narrowband filter ($NB < 23.5$), are located above the 5 σ color excess line, and have an observed EW greater than 125 Å. We can detect galaxies with emission-line strengths brighter than 1.4×10^{-16} ergs cm^{-2} s^{-1}. This flux limit corresponds to a Lyα luminosity of $1.9 \times 10^9\ L_\odot$. Thirty-seven spatially resolved *NB* excess objects are detected. Table 2 lists the positions and measured properties of these objects.

In addition, seven unresolved objects with *UBV* colors consistent with QSOs (e.g., Hall et al. 1996a, 1996b) are detected in emission with equivalent widths greater than 30 Å in the observed frame. Table 3 lists the positions and measured properties of these objects.

Finally, a QSO at $z = 2.38$ was found by Hawkins (2000). We detect this object in emission, but it was not selected as a QSO candidate because the *UBV* colors are within the stellar locus. We include this QSO in Table 3.

3.1. *Foreground Contamination*

For spatially resolved narrowband excess sources, the only likely contaminating line is [O II] (3727 Å). Our narrowband filter centered at 4107 Å is sensitive to [O II] emission from

TABLE 2
EMISSION-LINE GALAXIES

α (J2000.0)	δ (J2000.0)	*NB* (mag)	*B*−*NB* (mag)	Lyα Flux (ergs cm^{-2} s^{-1})	EW$_0$ (Å)	Notes
21 40 19.98	−44 19 48.2	22.62	1.91	2.73×10^{-16}	380	
21 40 31.00	−44 36 04.5	22.97	1.53	1.81×10^{-16}	215	
21 40 33.10	−44 36 10.8	22.91	1.37	1.81×10^{-16}	169	
21 40 36.77	−44 20 28.8	23.20	1.78	1.56×10^{-16}	312	
21 40 48.09	−44 31 01.7	23.11	2.87	1.95×10^{-16}	3026	
21 40 48.97	−44 01 23.6	22.77	1.29	2.00×10^{-16}	150	
21 40 58.22	−44 00 22.0	23.00	3.00	2.18×10^{-16}	5900	
21 41 02.90	−44 01 55.9	22.81	1.25	1.89×10^{-16}	141	
21 41 07.38	−44 38 11.7	23.04	1.34	1.59×10^{-16}	162	
21 41 44.41	−44 37 06.7	22.68	1.82	2.54×10^{-16}	331	
21 41 47.66	−44 21 21.9	22.61	2.37	2.95×10^{-16}	824	
21 41 53.55	−44 38 18.3	23.18	1.82	1.60×10^{-16}	331	
21 42 06.03	−44 34 47.9	23.18	2.58	1.79×10^{-16}	1277	B6
21 42 14.28	−44 32 15.8	22.18	2.07	4.21×10^{-16}	489	
21 42 27.56	−44 20 30.1	20.97	2.47	1.35×10^{-15}	1004	B1
21 42 28.54	−44 32 38.5	23.20	2.44	1.73×10^{-16}	944	
21 42 29.73	−44 21 02.8	22.86	2.30	2.33×10^{-16}	723	B2
21 42 32.20	−44 20 18.6	22.90	2.53	2.30×10^{-16}	1141	B4
21 42 34.88	−44 27 06.2	21.80	3.00	6.95×10^{-16}	5900	B7
21 42 42.63	−44 30 09.0	21.20	3.00	1.14×10^{-15}	5900	
21 42 54.07	−44 14 39.7	22.93	1.37	1.78×10^{-16}	169	
21 42 56.34	−44 37 56.8	22.48	1.56	2.86×10^{-16}	225	
21 43 00.09	−44 19 21.7	22.57	1.70	2.73×10^{-16}	277	
21 43 03.57	−44 23 44.2	21.42	2.61	9.06×10^{-16}	1371	B5
21 43 03.80	−44 31 44.9	22.16	2.30	4.43×10^{-16}	723	
21 43 05.90	−44 27 21.0	21.06	2.10	1.19×10^{-15}	513	
21 43 06.42	−44 27 00.6	22.48	2.61	3.41×10^{-16}	1371	
21 43 11.48	−43 59 01.0	23.13	2.87	1.91×10^{-16}	3026	
21 43 22.22	−44 13 06.5	23.09	1.93	1.78×10^{-16}	392	
21 43 23.80	−44 41 36.4	22.87	1.79	2.12×10^{-16}	317	
21 43 24.06	−44 27 59.9	22.42	1.81	3.22×10^{-16}	326	
21 43 37.41	−44 17 53.4	23.21	2.51	1.73×10^{-16}	1092	
21 43 37.48	−44 23 52.8	22.65	2.47	2.88×10^{-16}	1004	
21 43 44.92	−44 05 46.3	22.53	1.66	2.81×10^{-16}	261	
21 43 48.30	−44 08 26.9	22.42	1.48	2.95×10^{-16}	200	
21 44 12.15	−44 05 46.6	21.46	2.41	8.56×10^{-16}	890	
21 44 12.97	−43 57 56.7	22.70	1.53	2.31×10^{-16}	215	

NOTE.—Units of right ascension are hours, minutes, and seconds, and units of declination are degrees, arcminutes, and arcseconds.

foreground $0.095 < z < 0.109$ galaxies. Indeed, we detect emission from many well-resolved spiral galaxies below our EW cutoff.

[O II] interlopers within our Lyα sample would have absolute *B* magnitudes around −13.8 and would hence be blue compact H II galaxies (BCGs). At this redshift, they would only be marginally spatially resolved, so we could not separate them from $z = 2.38$ Lyα emitters by morphology alone.

To be detected through our filter, they must lie within a box of comoving size $5.9 \times 5.9 \times 60$ Mpc and have a rest-frame [O II]

TABLE 3
EMISSION-LINE QSO CANDIDATES

α (J2000.0)	δ (J2000.0)	*NB* (mag)	*B*−*NB* (mag)	Line Flux (ergs cm^{-2} s^{-1})	EW$_0$ (Å)	*B*−*V* (mag)	*U*−*B* (mag)	Notes
21 40 52.46	−44 36 21.35	19.96	0.83	2.04E−15	70	0.26	−0.28	
21 41 54.50	−44 18 35.97	20.14	1.01	1.96E−15	96	0.05	−0.31	$z = 1.66$
21 42 35.12	−44 32 30.36	21.35	0.99	6.35E−16	93	0.36	−0.11	
21 42 43.49	−44 14 25.32	20.14	0.41	1.02E−15	27	0.07	−0.35	
21 43 16.44	−44 16 51.54	21.04	0.67	6.51E−16	51	0.08	−0.30	
21 43 20.38	−44 20 00.35	20.59	0.46	7.39E−16	31	0.06	−0.52	
21 43 22.53	−44 31 49.18	19.88	0.98	2.45E−15	91	0.04	−0.43	
21 43 26.25	−44 26 03.44	20.77	0.49	6.58E−16	34	0.26	−0.33	

NOTE.—Units of right ascension are hours, minutes, and seconds, and units of declination are degrees, arcminutes, and arcseconds.

equivalent width greater than 114 Å. Using the local luminosity function of Jerjen, Bingelli, & Freeman (2000), we would expect to find ~12 BCG galaxies in such a box. Pustilnik et al. (1999), however, found that only ~8% of BCG galaxies have [O II] equivalent widths large enough to meet our selection criteria. If this foreground region were an average one, we would therefore expect ~1 foreground BCG galaxy to be contaminating our sample.

The southernmost 80% of our field was included in the Las Campanas Redshift Survey (LCRS; Shectman et al. 1996), which has excellent sensitivity to large-scale structures at redshift $z \sim 0.1$. The region in which foreground [O II] emitters could contaminate our survey contains a single isolated cluster (A3800; Abell, Corwin, & Olowin 1989) but is otherwise empty of galaxies. The LCRS detects many filaments of galaxies at this redshift, but none lie in our field at redshifts that could cause [O II] emission to impersonate Lyα at $z = 2.38$. Despite the presence of A3800, the galaxy density is indeed slightly below the LCRS average at this redshift. A3800 is located 10′ west and 3′ south of our field center (see Fig. 4). We see no concentration of candidate Lyα-emitting galaxies at this location: indeed, quite the opposite. Only one of our candidates lies within 1 projected Mpc of this location. Three others lie around 1.3 projected Mpc from the cluster, but these are the three for which we have spectroscopic confirmation that they lie at $z = 2.38$. We therefore tentatively conclude that foreground contamination is unlikely to be a big problem.

Foreground contamination is more likely a problem for the seven narrowband excess QSO candidates. The narrowband excess could be caused by Lyα emission at redshift 2.38 but could also be quasars at other redshifts, with different lines producing the excess. Indeed, one of these sources was found (Francis et al. 1997) to be a QSO at $z = 1.66$, with its C IV (1549 Å) emission producing the narrowband excess. The luminosity and redshift distribution of QSOs implies that about 60%, or four, of these quasars should be Lyα emitters at redshift 2.38 (see Palunas et al. 2000). If some of these sources are QSOs at redshift 2.38, it will be further evidence that QSOs lie in the most massive dark matter halos, which in turn exist in the most highly clustered environments (e.g., Silk & Weinberg 1991).

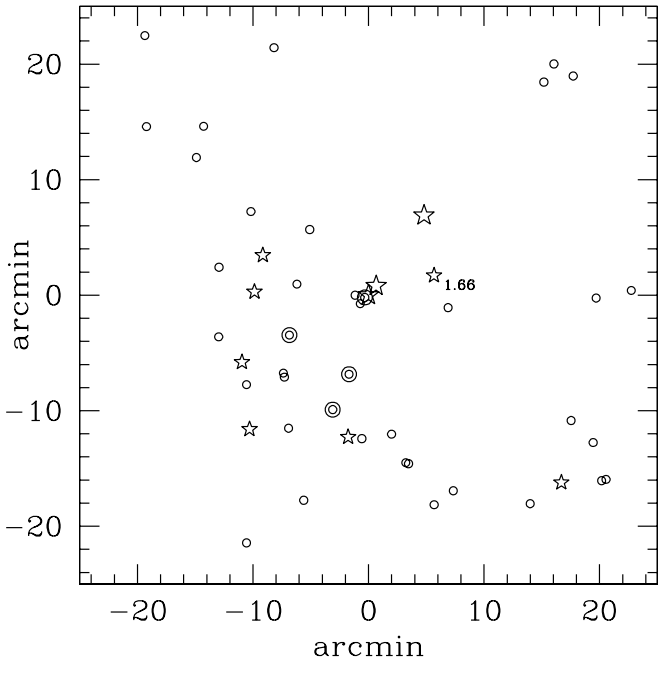

FIG. 4.—Distribution of emission-line objects in the field. The small open circles represent emission-line galaxy candidates. The large open circles are extended emission-line nebulae (blobs). The large open stars are the three known damped Lyα absorbers, and the small open stars are quasar candidates at the cluster redshift or lower redshifts. North is up, and east is to the left.

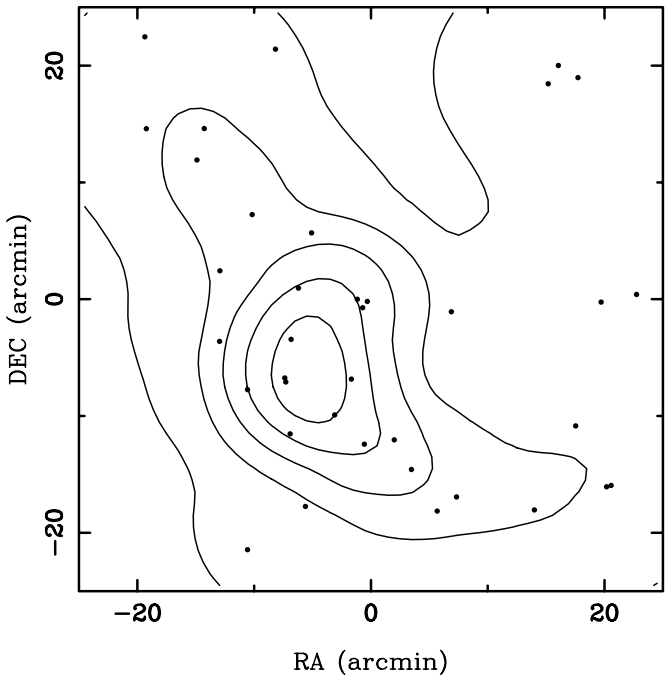

FIG. 5.—Density contours for the distribution of Lyα candidates estimated with the adaptive kernel routine. The lowest contour is one galaxy per resolution element 3.3×10^{-3} galaxies arcmin^{-2}. The highest contour is 5.7×10^{-2} galaxies arcmin^{-2}.

4. DISCUSSION

4.1. *The Space Density of Lyα Emitters*

We are sensitive to Lyα-emitting galaxies over a $45' \times 45'$ field minus $9' \times 9'$ in the southeast corner, in the redshift range $2.356 < z < 2.401$. For our adopted cosmology, this corresponds to a volume of 6100 comoving Mpc^2 in area and 59 comoving Mpc deep. Figure 5 shows the density contours of Lyα candidates estimated using an adaptive kernel routine (Beers et al. 1990). The initial smoothing scale is 12′. The highest density contour is 5.7×10^{-2} sources per square arcminute, corresponding to a spatial density of 3.0×10^{-4} sources per cubic Mpc. The average density over the whole field is 1.9×10^{-2} sources per square arcminute, corresponding to a spatial density of 1×10^{-4} sources per cubic Mpc.

Steidel et al. (2000) surveyed 20,000 cubic comoving Mpc at redshift 3.09, targeting a cluster of Lyα dropout galaxies. Their survey was sensitive to lower Lyα luminosities than ours, and they used a lower rest-frame equivalent-width threshold. They find nine candidates meeting our luminosity and equivalent-width thresholds corrected for redshift, yielding a density of 4.5×10^{-4} sources per cubic Mpc. Steidel et al. (2000) calculate that this space density is a factor of 6.0 ± 2.4 greater than that of smaller survey of Cowie & Hu (1998). This implies that peak density in our field is a factor of 4 overdense.

4.2. *Star Formation Rates*

To estimate the star formation rate, we first assume that star formation powers the observed Lyα flux. This is almost certainly a great underestimate: even tiny amounts of dust will greatly reduce the observed Lyα flux because of its high optical depth. We use an unreddened Lyα/Hα ratio of 8 : 1 and the conversion factor between Hα flux and star formation rate of Kennicutt (1983). Our faintest candidates ($NB = 23.25$) have inferred star formation rates of $\sim 9\ M_\odot\ \mathrm{yr}^{-1}$.

Summing over all galaxies down to our flux limit, and making a crude correction for incompleteness among the faintest, the integrated star formation rate density (assuming no dust obscuration) is $2.4 \times 10^{-3}\ M_\odot\ \mathrm{Mpc}^{-3}\ \mathrm{yr}^{-1}$, well below the value ($\sim 0.1\ M_\odot\ \mathrm{Mpc}^{-3}\ \mathrm{yr}^{-1}$) derived from integrated blue light by Madau, Pozzetti, & Dickinson (1998).

We also estimate the star formation rate from the 1600 Å UV continuum using the Madau et al. (1998) formula. At $z = 2.38$, the 1600 Å continuum falls in the V band. We detect 23 of our candidates in the V band. The star formation density implied by these candidates is $5 \times 10^{-3}\ M_\odot\ \mathrm{Mpc}^{-3}\ \mathrm{yr}^{-1}$. The star formation rate for a candidate at the V-band limit of 25.3 mag is $\sim 18\ M_\odot\ \mathrm{yr}^{-1}$. The 14 galaxies not detected in the V band could add, as an upper limit, $0.6 \times 10^{-3}\ M_\odot\ \mathrm{Mpc}^{-3}\ \mathrm{yr}^{-1}$ to the star formation rate density. Our Lyα candidates therefore contribute only a small fraction ($\sim 5\%$) of the overall star formation rate density at $z = 2.38$.

In a detailed study of the spectra of Lyman break galaxies, Shapley et al. (2003) conclude that galaxies with the strongest Lyα emission have bluer UV continua, weaker interstellar absorption, and smaller star formation rates than galaxies with weak Lyα emission or Lyα absorption. Lyα emission from galaxies with the highest star formation rates is absorbed by dust.

4.3. *The Distribution of Lyα Emission Candidates*

The distribution of our candidate-resolved Lyα-emitting sources is shown in Figure 4. There is no obvious overdensity surrounding the previously known cluster at the field center. Instead, most of the candidates lie in a broad band extending from the northeast of the field to the south. There is a significant lack of galaxies in the north and west. These regions have long integration times. There are three close pairs or triplets of candidates, but otherwise the candidates are well spaced. The pairs have a spacing of about 20″ or a minimum separation of 200 proper kpc. The spacing of the galaxies in the triplet is about 50″ or a minimum separation of 440 proper kpc.

4.3.1. *Comparison to a Random Distribution*

We used two statistics to compare our data to a random distribution. We compare these statistics to results from Monte Carlo simulations generated with the same exposure time mask. In this section we show that the distribution of our candidates has a significant excess of close (<1′) pairs and of large (6′–8′) voids.

The first statistic is essentially the angular two-point correlation function. For a series of angular separations, we take each data point in turn and count the number of other data points within that angular radius.

The second statistic is a two-dimensional analog of the void probability function (VPF). For each angular scale, we randomly place 1000 circles with that radius on our field, so that the circles do not extend beyond the edge of our data. We count the fraction of these circles that did not contain any data points. The requirement that the circles not extend beyond the edge of the data makes this statistic most sensitive to voids near the center of the field. VPFs are sensitive to structures such as voids and filaments, to which the two-point correlation function is relatively insensitive.

Our data were compared to random Monte Carlo simulations generated as follows. At each location in our image, the total exposure time was calculated. Using these total exposure times, the relative flux limits in every part of our field were computed. The number/magnitude distribution of our brighter candidates can be reasonably approximated as a power law, with the number per unit magnitude increasing by a factor of roughly 5. Combining this number-magnitude relation with the flux limits, we calculated the relative probability of finding a candidate per unit area in any given part of our image. We then used this relative probability map to generate 2000 fake data sets, each containing the same number of sources as the real data.

Our data have a significant excess of galaxies with separations less than 1′. Only 0.1% of the Monte Carlo simulations produced this many close galaxies. On larger scales, our data still show an excess of galaxies, but this is no longer significant at the 5% level.

The VPF (Fig. 6) is more interesting. There is a clear excess of voids on scales of 5′ or greater. On scales of 5′–8′, this excess is significant at the 99.9% confidence level (i.e., fewer than 0.1% of our randomly generated data sets had VPFs as large as our data).

We conclude that there is a significant excess of voids, and of small-scale clustering, in our data. This conclusion is insensitive to the details of how we generated the random data sets: changes in (for example) the assumed number/magnitude relation made little difference to our results.

4.3.2. *Comparison with ΛCDM N-Body Simulations*

The distribution of our Lyα candidates is thus inconsistent with a random distribution, with 99.5% confidence. Assuming that they are indeed galaxies at redshift 2.38, is their distribution consistent with theoretical predictions? In this section, we show that while the two-point correlation coefficient of our galaxy candidates is quite consistent with the predictions of a ΛCDM simulation, the distribution of our candidates shows more voids on 6′–8′ scales, with 97% confidence.

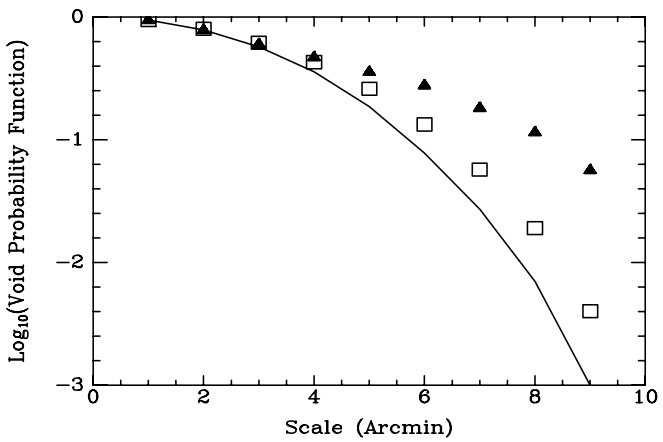

FIG. 6.—Void probability function of our data (*filled triangles*) compared to the average VPFs of randomly distributed points (*solid line*) and VPFs derived from the ΛCDM *n*-body simulations (*open squares*).

To evaluate the apparent excess of voids, we compared our measured distribution of galaxies against the ΛCDM *n*-body simulations performed by the VIRGO consortium (Kauffmann et al. 1999). We used their galaxy catalog, generated for redshift 2.12. For each galaxy, they list its position, stellar mass, gaseous mass, and star formation rate.

Mock catalogs were generated as follows. Our observations were targeted at the source B1, a probable pair of giant elliptical galaxies surrounded by an extensive neutral hydrogen cloud (Francis et al. 2001b). B1 has an estimated stellar mass of $10^{10.9}\ M_\odot$ and gaseous mass of $10^{9.7}\ M_\odot$. We picked five galaxies in the ΛCDM simulations that had stellar and gaseous masses at least this large and that lay far enough from the edge of the simulation volume. The regions around these "B1-analog" galaxies should be good matches to our data. For comparison, we also picked eight random locations within the ΛCDM simulation volume. We then extracted the galaxies that lay within a volume $70 \times 70 \times 46$ comoving Mpc (for our adopted cosmology) centered at each of these locations. There were 180 ± 30 ($1\ \sigma$) galaxies in their catalogs in each of these volumes.

We then had to sparsely sample the galaxies within each of these volumes to generate mock catalogs with (1) 37 galaxies and (2) a probability of being detected consistent with our exposure time map. We did this in three different ways.

1. *Randomly.*—As Lyα emission can be generated in many ways (by star formation, shocks, cooling flows, active galactic nuclei [AGNs], etc.), and its escape in measurable quantities depends on accidents of the geometry and dust distribution inside galaxies, we first assumed that all the galaxies in the ΛCDM simulations had the same probability ($37/180 \sim 20\%$) of being detected by our survey.

2. *Star formation rate.*—If the Lyα flux is generated by star formation, only galaxies with star formation rates in excess of $8\ M_\odot\ \mathrm{yr}^{-1}$ would have been detected. We therefore took only galaxies with star formation rates at least this large and generated random subsamples with the correct size and probability of detection as a function of position in our field. Only 25% of the galaxies within the ΛCDM cubes had star formation rates this large.

3. *Mass.*—We took only galaxies with masses greater than $10^{10.3}\ M_\odot$, once again picking random subsamples of the appropriate size and with probabilities of detection scaling appropriately with exposure time in each part of our image.

For each data cube, and for each of these three subsampling techniques, we repeated the random subsampling 2000 times. We then calculated the angular two-point correlation function and the VPF for each subsampling of each data cube and compared our results with the observations.

Figure 7 shows our data and five of the mock ΛCDM data cubes (centered on the five B1-analog galaxies). The cubes shown have been randomly subsampled: those sampled on the basis of star formation rate or mass look very similar. Figure 6 shows the average VPF of the randomly subsampled data cubes (centered on B1-analog galaxies).

The angular two-point correlation coefficient of our data and of the ΛCDM simulations are in excellent agreement. As Figure 6 shows, however, the agreement is not as good for the VPF. Our data have a VPF considerably higher than that of the simulations on large scales.

Is this difference significant? The VPFs of our 13 simulated data cubes (five centered on B1-analog galaxies and eight randomly located) actually showed rather little scatter when averaged over all the 2000 random subsamplings of each. The dominant source of scatter was the selection of the 37 galaxies in each simulated volume, which was typically twice as large. Our uncertainty is thus dominated by the small sample size rather than by cosmic variance.

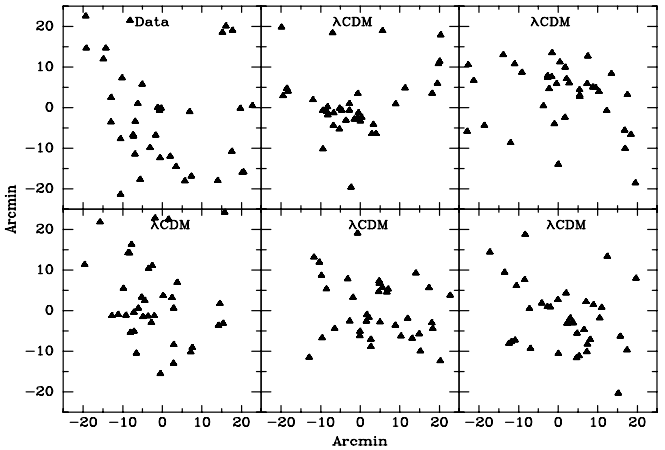

FIG. 7.—Distribution on the sky of our candidate Lyα-emitting galaxies (*top left*) compared to five simulated data sets drawn from the ΛCDM *n*-body simulations. These simulations use random subsampling and are centered on B1-analog galaxies.

If we take the five data cubes centered on B1-analogs, and generate 2000 random subsamplings of each, fewer that 0.1% of all these random subsamplings have VPFs as large as we observe on scales of 5′–8′. If we subsample on the basis of star formation rate or galaxy mass, this fraction rises to around 1%. We would expect this, as more massive galaxies and those with larger star formation rates, are expected to be more strongly biased. If we repeat these calculations for the randomly centered data cubes, the VPF also rises slightly. This is presumably because centering our data cube on a B1 analog precludes the possibility of a void in the center of the field.

Thus, the observed distribution of galaxies has an excess of voids over the ΛCDM simulations, significant at roughly the 99% level. A qualitative impression of this can be gained from Figure 7. While all the ΛCDM simulations show empty regions near the edge of the field, this is an artifact of the shorter exposure times in these regions. The simulations do not show large voids in the central $\pm 13'$. Because of the restriction that we only place voids so that they do not overlap the edges of our field, our VPF statistic is mostly sensitive to the distribution of galaxies in this central region.

4.3.3. *Discussion of the Voids*

We thus have tentative evidence from our survey of larger voids in the galaxy distribution at redshift 2.38 than predicted by one particular ΛCDM simulation. With only 97% confidence, a sample size of 34 and no spectral confirmation for most of our candidate galaxies, this evidence must be regarded as tentative at best. But if it is confirmed by larger samples, what is it telling us?

Steidel et al. (2000) did not see voids, but they covered too small a region on the sky to be sensitive to the scales of void we are detecting. Ouchi et al. (2003) imaged a region $\sim$25% the size of ours, searching for Lyα candidates at $z = 4.86$. Voids can be seen in their data if only the brightest objects are

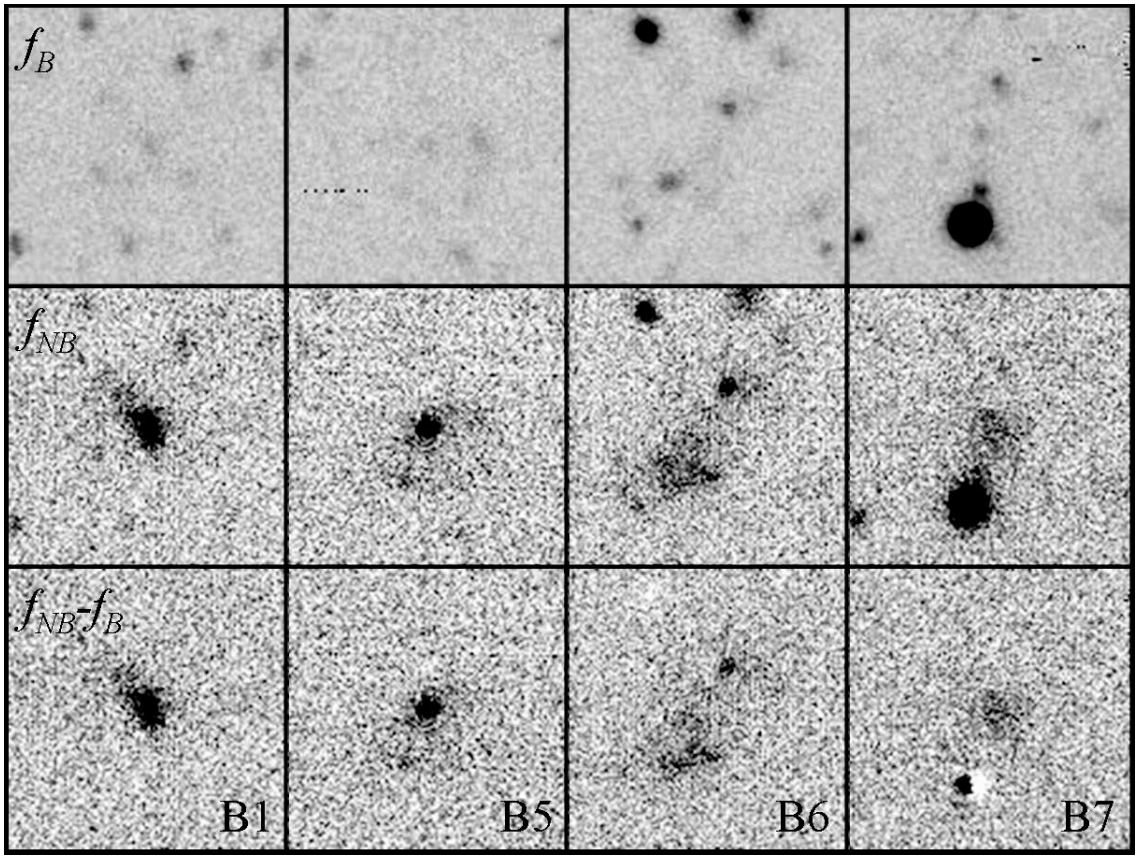

FIG. 8.—Images of the blobs. The top row shows the broadband image of each blob, the middle row shows the narrowband image, and the bottom row shows the difference between the two, scaled to give an image of the Lyα emission. Each image is $30'' \times 30''$.

selected so that their number per unit area matches ours. Voids might also explain the enormous field-to-field variance in the space density of Lyα sources found by Pascarelle, Windhorst, & Keel (1998). The spiky distribution of the redshifts of Lyman dropout galaxies seen by Steidel et al. (1998) and Adelberger et al. (1998) would also be consistent with large voids in the high-redshift galaxy distribution.

If the distribution of galaxies really contains more 10 comoving Mpc scale voids than predicted, either the ΛCDM is predicting too uniform a distribution of galaxies, or the voids contain dark matter halos, which for some reason do not contain detectable galaxies.

There is some evidence for the latter hypothesis. The sight line to background QSO 2138−4427 passes through one of the voids in our data, but the QSO spectrum shows a metal-enriched damped Lyα absorption system at our redshift (Francis & Hewett 1993; Francis, Wilson, & Woodgate 2001a). So there is clearly at least one dense concentration of gas and some stars within one of our voids.

4.4. *Blobs*

Some high-redshift galaxy clusters contain extended Lyα emission nebulae, or "blobs" (Steidel et al. 1998). The blobs are radio-quiet ($<$140 μJy at 1.4 GHz) but otherwise share morphological similarity with the nebulae around radio galaxies (e.g., Kurk et al. 2001). Lyα blobs are large, bright gas clouds ($\sim$100 h^{-1} kpc, $\Omega_m = 0.3, \Omega_\Lambda = 0.7$; Ly$\alpha$ flux up to $1.8 \times \sim 10^{-15}$ ergs cm^{-2} s^{-1}). They appear to be common in regions of significant galaxy overdensity ($\sim$10 times that of the field) at high redshift. Most blobs are associated with a host galaxy, although not symmetrically centered on it. Blobs may break into smaller knots of Lyα and continuum emission, with velocity differences of $\Delta V \lesssim 2000$ km s^{-1} (Steidel et al. 2000). Blobs can be among the brightest high-z submillimeter sources (Chapman et al. 2001). Some blobs (Francis et al. 2001b) show C IV emission (and may host AGNs), but others do not.

We detect four Lyα blobs in the narrowband image. One of these, "B1," has previously been detected (Francis et al. 2001b). Figure 8 shows the broad and narrowband images of each blob, together with the continuum-subtracted emission-line image. Each blob conforms to the expected size and brightness of this class of object. Table 4 summarizes the characteristics of the blobs.

These blobs may be pregalactic clouds of gas, in the process of initial collapse, or destined to be stripped away into the intracluster medium (ICM). In the blobs, we may witness a stage of structure formation that is illuminated by an unusual or transitory phenomenon. The excitation mechanism for the Lyα emission is not known, but three primary models have been suggested:

In the early stages of a galaxy's formation, gas collapses into the dark matter potential well and cools via radiation (e.g., Fabian et al. 1986). Haiman, Spaans, & Quataert (2000) calculate that cooling flows (with gas temperatures of a few times 10^4 K) could produce the observed flux range, size, surface brightness profiles, and number density observed from Lyα blobs. While Fardal et al. (2000) doubt that cooling

TABLE 4
Lyα Blobs

Name	Redshift (z)	Major Axis (arcsec)	Lyα Flux (ergs cm^{-2} s^{-1})	C IV Emission	References
SB-1	3.09	17	1.4×10^{-15}	No	1, 2
SB-2	3.09	15	1.2×10^{-15}	No	1, 2
KB-A	2.39	~ 8	1.1×10^{-15}	Yes	3, 4
KB-B	2.39	~ 8	0.45×10^{-15}	Yes	3, 4
B1	2.38	17	1.8×10^{-15}	Yes	5, 6
B5	2.38	8	1.5×10^{-15}	...	6
B6	2.38	8	1.4×10^{-15}	...	6
B7	2.38	7	0.7×10^{-15}	...	6

References.—(1) Steidel et al. 2000; (2) Bautz & Garmire 2001; (3) Windhorst, Keel, & Pascarelle 1998; (4) Keel et al. 1999; (5) Francis et al. 2001b; (6) this work.

flows would have sufficient luminosity, Francis et al. (2001b) suggest that shocks within the infalling gas can trigger the blob emission in the cooling flow. Confirmation that the blobs are high-redshift cooling flows would have profound implications for the interpretation of semianalytic galaxy formation models (e.g., Fall & Efstathiou 1980), since we would be observing the initial collapse of gas into dark matter potential wells.

Taniguchi, Shioya, & Kakazu (2001 and references therein) suggest that starburst-powered winds trigger Lyα emission in the expelled gas. Dust could obscure the host galaxy, with the Lyα emission arising from a superwind extending $\sim$100 kpc from the host. The dusty host galaxies would eventually evolve into ordinary elliptical galaxies, and the blobs would presumably dissipate into the intracluster medium. The SCUBA detections support this model, implying rapid star formation (Chapman et al. 2001) and a probability of hosting an AGN (Barger et al. 2001). Superwinds would indicate that the blobs are the next phase of galaxy evolution after the initial collapse. Taniguchi & Shioya (2000) estimate this phase would last only 0.1 Gyr, occurring after the first 0.5 Gyr of star formation. The expelled gas would eventually be stripped into the ICM, although it would be metal-enriched, having been processed by supernovae in the host galaxy.

An AGN may photoionize the gas, similar to radio galaxy nebulae and Seyfert 2 galaxies with extended emission-line regions (e.g., Villar-Martin, Tadhunter, & Clark 1997). For example, a Lyα nebula has been found around the Hubble Deep Field–South QSO that is radio-quiet (Bergeron et al. 1999; Palunas et al. 2000). For the blobs, we do not see a strong UV continuum source; however, there may be an AGN surrounded by an obscuring torus (e.g., Krolik & Begelman 1986). In fact, most of the *Chandra* point sources do not show optical evidence for AGNs (Mushotzky et al. 2000). Assuming an ionization parameter of 10 and a density of 1 cm^{-3} at a distance of 10 kpc, a central source with luminosity 9×10^{45} ergs s^{-1} is required to ionize a Lyα blob with $L_X \sim 10^{44}$ ergs s^{-1}. The gas in AGN-supported blobs would contribute to the ICM, but with potentially lower metallicity than that from a starburst, thus diluting rather than enriching the ICM.

5. SUMMARY

Narrowband imaging in the J2143−4423 region has revealed 34 candidate Lyα emitters, including three new extended Lyα blob candidates and five possible quasars. Together with the previously reported emission-line galaxies and damped Lyα absorption systems, these detections suggest this field is one of the most highly evolved structures detected at high redshift.

The distribution of the candidates is nonrandom. There are more closely grouped galaxies, and more voids in the distribution, than would be expected from either a random distribution of galaxies or from the ΛCDM simulations of Kauffmann et al. (1999). This may indicate some environmental dependence on whether a galaxy emits detectable Lyα emission.

The detection of too many voids in our data is suggestive, but further observations with much more uniform sensitivity over much wider fields, combined with follow-up spectroscopy, will be required to definitively measure the topology of the distribution of high-redshift galaxies.

We thank K. Weaver and R. Mushotzky for useful discussions and the VIRGO consortium for making the outputs of their *n*-body simulations publicly available. We thank the referee, W. Keel, for comments, which improved the manuscript. This study was funded by a NASA grant NRA-98-03-UVG-011. The Cerro Tololo Inter-American Observatory (CTIO) is operated by the Association of Universities for Research in Astronomy (AURA), Inc., under cooperative agreement with the National Science Foundation. This work was supported by the Space Telescope Imagining Spectrograph (STIS) Investigation Definition Team (IDS) through the National Optical Astronomical Observatories and by the Goddard Space Flight Center.

REFERENCES

Abell, G. O., Corwin, H. G., & Olowin, R. P. 1989, ApJS, 70, 1
Adelberger, K. L., Steidel, C. C., Giavalisco, M., Dickinson, M., Pettini, M., & Kellogg, M. 1998, ApJ, 505, 18
Barger, A. J., Cowie, L. L., Mushotzky, R. F., & Richards, E. A. 2001, AJ, 121, 662
Bautz, M. W., & Garmire, G. P. 2001, AAS Meeting, 199, 10010
Beers, T. C., Flynn, K., & Gebhardt, K. 1990, AJ, 100, 32
Bergeron, J., Petitjean, P., Cristiani, S., Arnouts, S., Bresolin, F., & Fasano, G. 1999, A&A, 343, L40
Bertin, E., & Arnouts, S. 1996, A&AS, 117, 393
Campos, A., Yahil, A., Windhorst, R. A., Richards, E. A., Pascarelle, S., Impey, C., & Petry, C. 1999, ApJ, 511, L1
Chapman, S. C., Lewis, G. F., Scott, D., Richards, E., Borys, C., Steidel, C. C., Adelberger, K. L., & Shapley, A. E. 2001, ApJ, 548, L17

Cowie, L. L., & Hu, E. M. 1998, AJ, 115, 1319
Ellingson, E., Yee, H. K. C., & Green, R. F. 1991, ApJ, 371, 49
Fabian, A. C., Arnaud, K. A., Nulsen, P. E. J., & Mushotzky, R. F. 1986, ApJ, 305, 9
Fall, S. M., & Efstathiou, G. 1980, MNRAS, 193, 189
Fardal, M. A., Katz, N., Gardner, J. P., Hernquist, L., Weinberg, D. H., & Davé, R. 2001, ApJ, 562, 605
Francis, P. J., & Hewett, P. C. 1993, AJ, 105, 1633
Francis, P. J., Wilson, G. M., & Woodgate, B. E. 2001a, Publ. Astron. Soc. Australia, 18, 64
Francis, P. J., Woodgate, B. E., & Danks, A. C. 1997, ApJ, 482, L25
Francis, P. J., et al. 1996, ApJ, 457, 490
———. 2001b, ApJ, 554, 1001
Geller, M. J., & Huchra, J. P. 1989, Science, 246, 897
Giavalisco, M., Steidel, C. C., Adelberger, K. L., Dickinson, M. E., Pettini, M., & Kellogg, M. 1998, ApJ, 503, 543
Haiman, Z., Spaans, M., & Quataert, E. 2000, ApJ, 537, L5
Hall, P. B., Osmer, P. S., Green, R. F., Porter, A. C., & Warren, S. J. 1996a, ApJ, 462, 614
———. 1996b, ApJ, 471, 1073
Hawkins, M. R. S. 2000, A&AS, 143, 465
Hogg, D. W., et al. 1998, AJ, 115, 1418
Hu, E. M., & McMahon, R. G. 1996, Nature, 382, 281
Jerjen, H., Bingelli, B., & Freeman, K. C. 2000, AJ, 119, 593
Kauffmann, G., Colberg, J. M., Diaferio, A., & White, S. D. M. 1999, MNRAS, 303, 188
Kauffmann, G., Nusser, A., & Steinmetz, M. 1997, MNRAS, 286, 795
Keel, W. C., Cohen, S. H., Windhorst, R. A., & Waddington, I. 1999, AJ, 118, 2547
Kennicutt, R. C., Jr. 1983, ApJ, 272, 54
Krolik, J. H., & Begelman, M. C. 1986, ApJ, 308, L55
Kron, R. G. 1980, ApJS, 43, 305
Kurk, J. D., Pentericci, L., Røttgering, H. J. A., & Miley, G. K. 2001, Ap&SS Suppl., 277, 543
Landolt, A. U. 1992, AJ, 104, 340
Madau, P., Pozzetti, L., & Dickinson, M. 1998, ApJ, 498, 106
Mo, H. J., Mau, S., & White, S. D. M. 1999, MNRAS, 304, 175
Møller, P., & Fynbo, J. U. 2001, A&A, 372, L57
Mushotzky, R. F., Cowie, L. L., Barger, A. J., & Arnaud, K. A. 2000, Nature, 404, 459
Ouchi, M., et al. 2003, ApJ, 582, 60
Palunas, P., et al. 2000, ApJ, 541, 61
Pascarelle, S. M., Windhorst, R. A., & Keel, W. C. 1998, AJ, 116, 2659
Pustilnik, S. A., Engels, D., Ugryumov, A. V., Lipovetsky, V. A., Hagen, H.-J., Kniazev, A. Y., Izotov, Y. I., & Richter, G. 1999, A&AS, 137, 299
Rhoads, J. E. 2000, PASP, 112, 703
Schlegel, D. J., Finkbeiner, D. P., & Davis, M. 1998, ApJ, 500, 525
Shapley, A. E., Steidel, C. C., Pettini, M., & Adelberger, K. L. 2003, ApJ, 588, 65
Shectman, S. A., Landy, S. D., Oemler, A., Tucker, D. L., Huan, L., Kirshner, R. P., & Schechter, P. L. 1996, ApJ, 470, 172
Silk, J., & Weinberg, D. 1991, Nature, 350, 272
Steidel, C. C., Adelberger, K. L., Dickinson, M., Giavalisco, M., Pettini, M., & Kellogg, M. 1998, ApJ, 492, 428
Steidel, C. C., Adelberger, K. L., Shapley, A. E., Pettini, M., Dickinson, M., & Giavalisco, M. 2000, ApJ, 532, 170
Steidel, C. C., Giavalisco, M., Pettini, M., Dickinson, M., & Adelberger, K. L. 1996, ApJ, 462, L17
Taniguchi, Y., & Shioya, Y. 2000, ApJ, 532, L13
Taniguchi, Y., Shioya, Y., & Kakazu, Y. 2001, ApJ, 562, L15
Teplitz, H. I, Malkan, M. A., & McLean, I. S. 1998, ApJ, 506, 519
Villar-Martin, M., Tadhunter, C., & Clark, N. 1997, A&A, 323, 21
White, S. D. M., & Frenk, C. 1991, ApJ, 379, 52
Windhorst, R. A., Keel, W. C., & Pascarelle, S. M. 1998, ApJ, 494, L27